Electronic Supplementary Material (ESI) for Journal of Materials Chemistry A.

Supporting Information

High performance planar perovskite solar cells with a perovskite of mixed organic cations and mixed halides, $MA_{1-x}FA_xPbI_{3-y}Cl_y$

Table S1. Photovoltaic performances of $MA_{1-x}FA_xPbI_{3-y}Cl_y$-based PSCs with different *x* values.

Perovskite	Precursors	Perovskite film thickness (nm)	Annealing duration (min)-temperature (°C)	J_{sc}[a] (mA/cm^2)	V_{oc}[a] (V)	*FF*[a]	PCE[a] [best (average)] (%)
$MA_{0.90}FA_{0.10}PbI_{3-y}Cl_y$	1.26 M PbI_2, 0.14 M $PbCl_2$, 1.215 M MAI, 0.135 M FAI	~280	15-100	19.58 ±0.76	1.105 ±0.015	0.74 ±0.02	16.84 (16.00)
$MA_{0.85}FA_{0.15}PbI_{3-y}Cl_y$	1.26 M PbI_2, 0.14 M $PbCl_2$, 1.1475 M MAI, 0.2025 M FAI	~280	15-100	20.42 ±0.59	1.100 ±0.010	0.75 ±0.02	17.41 (16.78)
$MA_{0.80}FA_{0.20}PbI_{3-y}Cl_y$	1.26 M PbI_2, 0.14 M $PbCl_2$, 1.08 M MAI, 0.27 M FAI	~280	15-100	21.55 ±0.55	1.100 ±0.010	0.75 ±0.02	18.14 (17.45)
$MA_{0.75}FA_{0.25}PbI_{3-y}Cl_y$	1.26 M PbI_2, 0.14 M $PbCl_2$, 1.0125 M MAI, 0.3375 M FAI	~280	15-100	20.46 ±0.54	1.090 ±0.010	0.75 ±0.02	17.74 (16.97)
$MA_{0.70}FA_{0.30}PbI_{3-y}Cl_y$	1.26 M PbI_2, 0.14 M $PbCl_2$, 0.945 M MAI, 0.405 M FAI	~280	15-100	20.26 ±0.64	1.080 ±0.010	0.75 ±0.02	16.68 (16.30)
$MA_{0.60}FA_{0.40}PbI_{3-y}Cl_y$	1.26 M PbI_2, 0.14 M $PbCl_2$, 0.81 M MAI, 0.54 M FAI	~280	15-100	20.12 ±0.45	1.060 ±0.010	0.76 ±0.02	16.48 (16.04)
$MA_{0.50}FA_{0.50}PbI_{3-y}Cl_y$	1.26 M PbI_2, 0.14 M $PbCl_2$, 0.675 M MAI, 0.675 M FAI	~280	15-100	20.00 ±0.45	1.050 ±0.010	0.67 ±0.02	14.73 (14.04)

[a] The average results are derived from 12 perovskite solar cells from two different batches.

Table S2. Photovoltaic performances of $MA_{0.80}FA_{0.20}PbI_{3-y}Cl_y$-based PSCs with the perovskite layer annealed at different temperatures.

Perovskite	Precursors	Perovskite film thickness (nm)	Annealing duration (min)-temperature (°C)	J_{sc}[a] (mA/cm^2)	V_{oc}[a] (V)	*FF*[a]	PCE[a] [best (average)] (%)
$MA_{0.80}FA_{0.20}PbI_{3-y}Cl_y$	1.26 M PbI_2, 0.14 M $PbCl_2$, 1.08 M MAI, 0.27 M FAI	~280	60-80	18.85 ±0.72	1.115 ±0.015	0.64 ±0.03	13.87 (13.16)
$MA_{0.80}FA_{0.20}PbI_{3-y}Cl_y$	1.26 M PbI_2, 0.14 M $PbCl_2$, 1.08 M MAI, 0.27 M FAI	~280	35-90	19.95 ±0.45	1.100 ±0.010	0.68 ±0.02	15.56 (14.94)
$MA_{0.80}FA_{0.20}PbI_{3-y}Cl_y$	1.26 M PbI_2, 0.14 M $PbCl_2$, 1.08 M MAI, 0.27 M FAI	~280	15-100	21.55 ±0.55	1.100 ±0.010	0.75 ±0.02	18.14 (17.45)
$MA_{0.80}FA_{0.20}PbI_{3-y}Cl_y$	1.26 M PbI_2, 0.14 M $PbCl_2$, 1.08 M MAI, 0.27 M FAI	~280	13-110	20.03 ±0.63	1.090 ±0.020	0.70 ±0.03	15.63 (15.22)
$MA_{0.80}FA_{0.20}PbI_{3-y}Cl_y$	1.26 M PbI_2, 0.14 M $PbCl_2$, 1.08 M MAI, 0.27 M FAI	~280	10-130	9.48 ±1.19	0.970 ±0.010	0.65 ±0.02	6.88 (6.11)
$MA_{0.80}FA_{0.20}PbI_{3-y}Cl_y$	1.26 M PbI_2, 0.14 M $PbCl_2$, 1.08 M MAI, 0.27 M FAI	~280	7-150	4.49 ±1.23	0.915 ±0.015	0.72 ±0.04	3.94 (2.99)

[a] Each average result is derived from 12 PSCs fabricated in two batches.

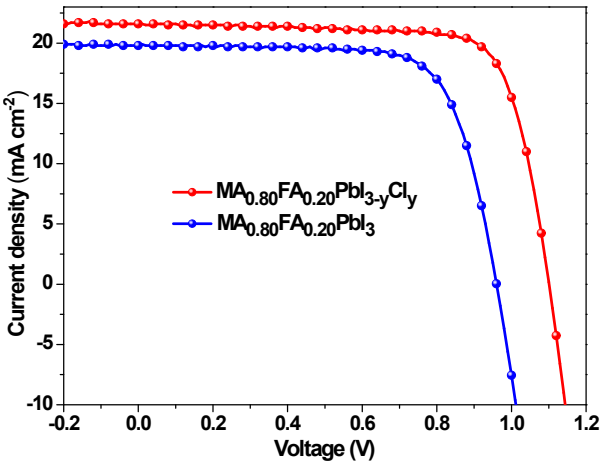

Fig. S1. *J-V* curves of ITO/PEDOT:PSS/perovskite/PCBM/C60/LiF/Ag PSCs with $MA_{0.80}FA_{0.20}PbI_{3-y}Cl_y$ and $MA_{0.80}FA_{0.20}PbI_3$ PSCs. The perovskite layers were annealed at 100 °C. The devices were tested under AM1.5G illumination (100 mW cm^{-2}). The *J-V* curves belong to the best performing devices amongst 12 PSCs fabricated in two batches.

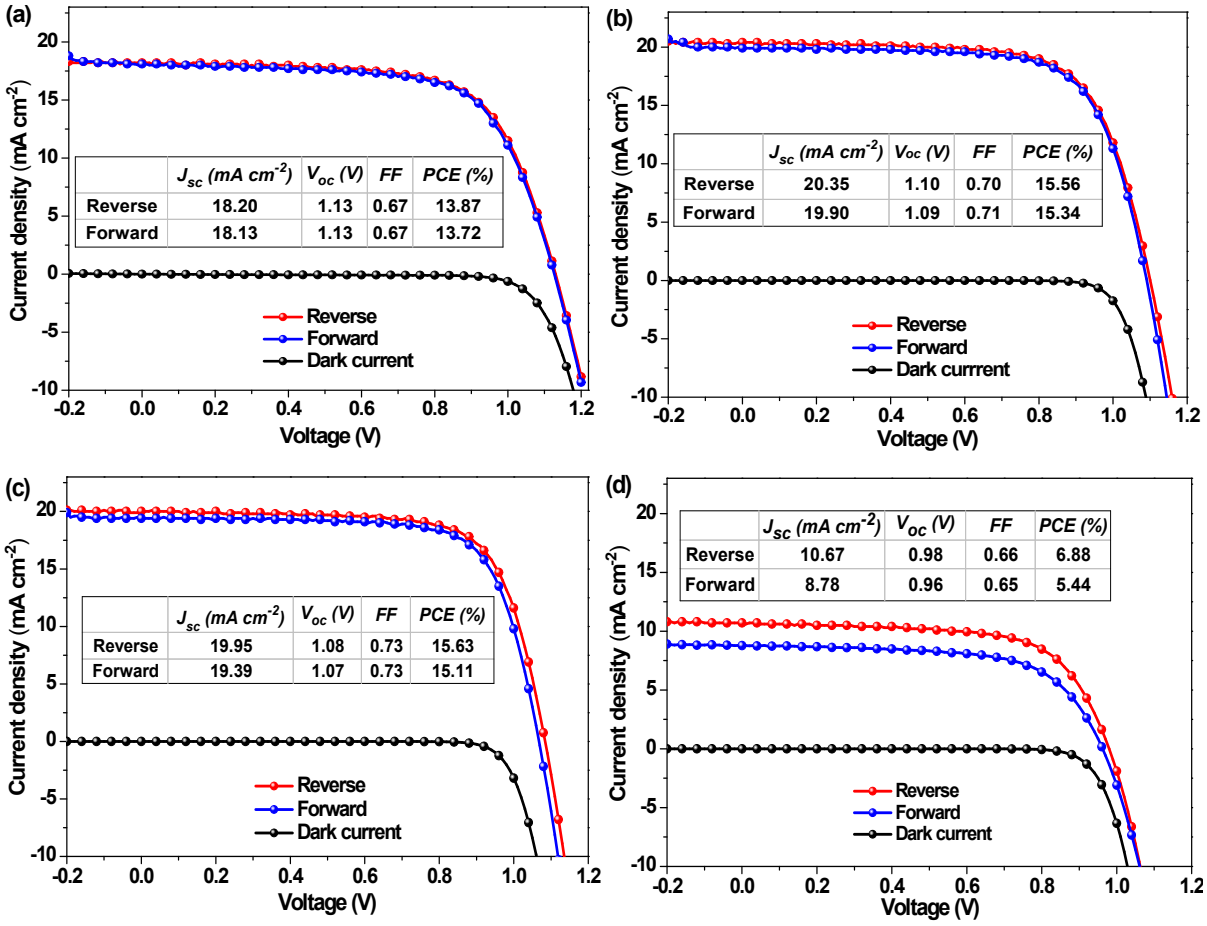

Fig. S2. *J-V* characteristics of ITO/PEDOT:PSS/$MA_{0.80}FA_{0.20}PbI_{3-y}Cl_y$/PCBM/C60/LiF/Ag PSCs with the $MA_{0.80}FA_{0.20}PbI_{3-y}Cl_y$ layer annealed at (a) 80 °C, (b) 90 °C, (c) 110 °C, and (d) 130 °C. The devices were tested under AM1.5G illumination (100 mW cm^{-2}). The *J-V* curves belong to the best performing devices amongst 12 PSCs fabricated in two batches.

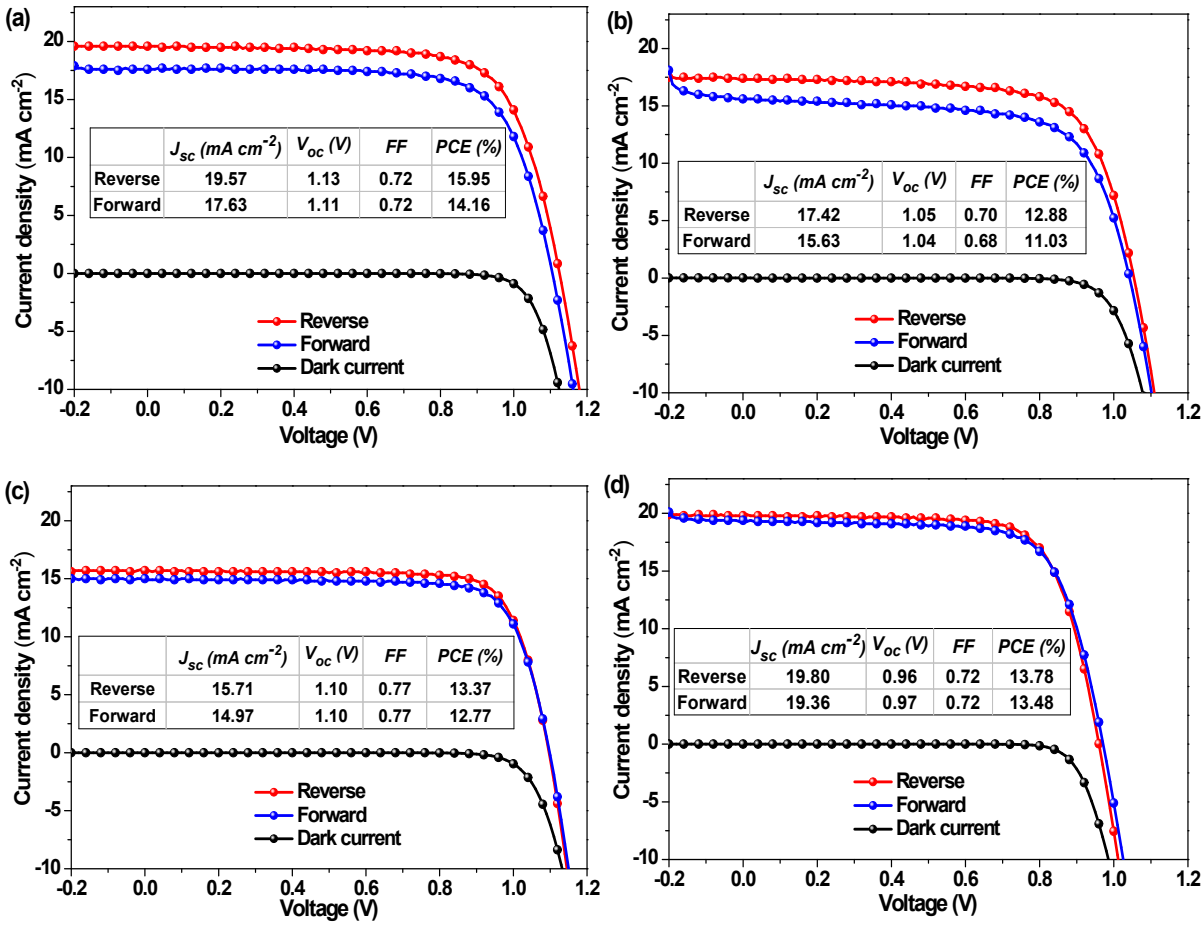

Fig. S3. *J-V* characteristics of ITO/PEDOT:PSS/perovskite/PCBM/C60/LiF/Ag PSCs with (a) $MAPbI_{3-y}Cl_y$, (b) $MAPbI_3$, (c) $MAPbI_{2.70}Br_{0.30}$, (d) $MA_{0.80}FA_{0.20}PbI_3$ PSCs. The devices were tested under AM1.5G illumination (100 mW cm^{-2}). The *J-V* curves belong to the best performing devices amongst 12 PSCs fabricated in two different batches.

Note S1. We also examined the hysteresis in the *J-V* curves of the PSCs employing the other active layers (Fig. S3). As it is evident from the *J-V* curves, considering perovskite morphology may not be sufficient to reveal the origin of electrical hysteresis in hybrid perovskites. For instance, $MAPbI_3$ composition with a R_{RMS} value of 7.2 nm seems to exhibit an electrical hysteresis; however, $MA_{0.80}FA_{0.20}PbI_{3-y}Cl_y$ PSC, which has slightly rougher thin film morphology (R_{RMS}= 10.7 nm), does not (Fig. 6). Besides, the incorporation of FA^+ into the hybrid perovskites is somehow beneficial for alleviating the anomalous hysteresis in hybrid perovskites. This can be observed when the *J-V* curves of the FA^+ inserted $MA_{0.80}FA_{0.20}PbI_{3-y}Cl_y$ and $MA_{0.80}FA_{0.20}PbI_3$ PSCs are compared with their non-FA^+ incorporating counterparts (Figs. S3 and 3). Thus; ferroelectricity, which is proposed to be another reason of the hysteresis, should be considered too. Understanding ferroelectricity in hybrid perovskites requires investigation of both the crystal symmetry and the incorporated organic cation. From the crystal structure point, for instance, the tetragonal phase of $MAPbI_3$ allows for a polar ferroelectric distortion, whereas this is not observed in the cubic phases of $MAPbBr_3$ or $MAPbCl_3$.[1] Hybrid perovskites also exhibit a molecular dipole due to the organic cation component, which can reorient freely on the picoseconds timescale. The organic cation component is not symmetric but it has a pseudo-spherical symmetry. Hence, it is claimed that existence of an electric field stabilizes a state in which the dipoles are aligned and the inorganic lattice is distorted. If this is correct, the hysteresis may depend on the magnitude of the dipole moment of the organic cation and its coupling to the halide cage. In this consideration, hysteresis and ferroelectricity correlation in hybrid perovskites incorporating different organic cations could be tested and compared.[1-3]

Eq. S1. Lattice parameters of the tetragonal perovskite phases are calculated by considering the (1,1,0) and (1,1,6) planes. The "d-spacings and Miller indices of tetragonal symmetry is:

$$\frac{1}{d^2} = \frac{h^2 + k^2}{a^2} + \frac{l^2}{c^2}$$

According to Bragg's Law:

$$2dsin\theta = n\lambda$$

Where; n is an integer, d is the spacing between the layers of atoms, λ is wavelength of the rays, and θ is the angle between the incident rays and the surface of the crystal.

Accordingly, the calculated "a" and "c" unit cell parameters of the tetragonal unit cell are summarized for the different perovskite compositions as below:

Composition	**2-Theta (°) (1,1,0 plane)**	**2-Theta (°) (1,1,6 plane)**	**a (nm)**	**c (nm)**
$MAPbI_3$	14.2101	43.2965	8.8073	12.5354
$MAPbI_{3-y}Cl_y$	14.2297	43.3555	8.7952	12.5192
$MAPbI_{2.70}Br_{0.30}$	14.2691	43.4933	8.7711	12.4814
$MA_{0.80}FA_{0.20}PbI_3$	14.1510	43.0997	8.8439	12.5899
$MA_{0.90}FA_{0.10}PbI_{3-y}Cl_y$	14.1707	43.2965	8.8317	12.5626
$MA_{0.80}FA_{0.20}PbI_{3-y}Cl_y$	14.1510	43.1194	8.8439	12.5844
$MA_{0.70}FA_{0.30}PbI_{3-y}Cl_y$	14.1313	43.0800	8.8562	12.5954
$MA_{0.60}FA_{0.40}PbI_{3-y}Cl_y$	14.1313	43.0407	8.8562	12.6063
$MA_{0.50}FA_{0.50}PbI_{3-y}Cl_y$	14.1117	42.9423	8.8684	12.6339

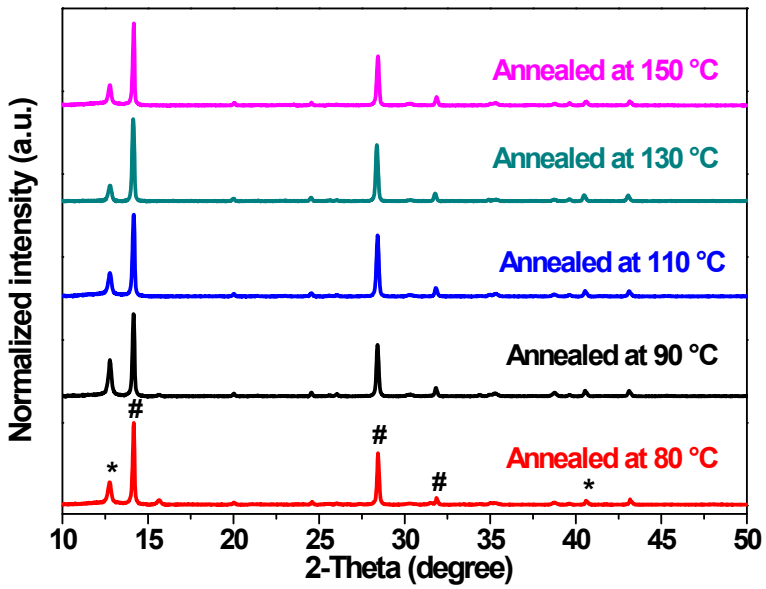

Fig. S4. XRD patterns of $MA_{0.80}FA_{0.20}PbI_{3-y}Cl_y$ films annealed at different temperatures. The corresponding PbI_2 (*) and perovskite peaks (#).

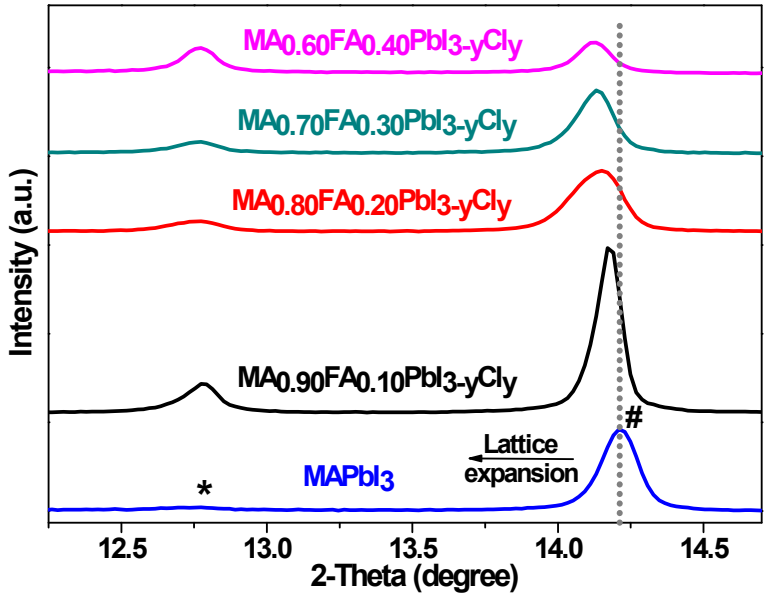

Fig. S5. XRD patterns of $MA_{1-x}FA_xPbI_{3-y}Cl_y$with different FA^+ mol ratios. The corresponding PbI_2 (*) and perovskite peaks (#).

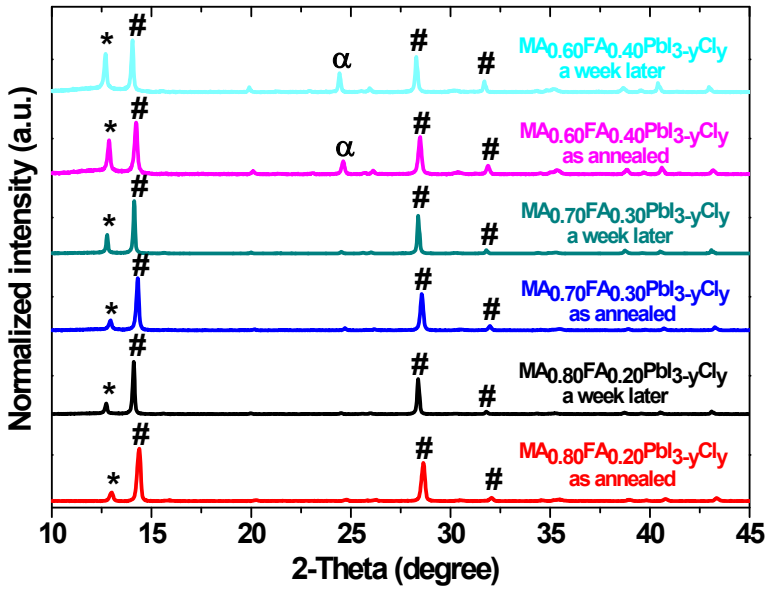

Fig. S6. XRD patterns of $MA_{0.80}FA_{0.20}PbI_{3-y}Cl_y$-as annealed (red), $MA_{0.80}FA_{0.20}PbI_{3-y}Cl_y$-a week later (black), $MA_{0.70}FA_{0.30}PbI_{3-y}Cl_y$-as annealed (blue), $MA_{0.70}FA_{0.30}PbI_{3-y}Cl_y$-a week later (dark cyan), $MA_{0.60}FA_{0.40}PbI_{3-y}Cl_y$-as annealed (magenta), and $MA_{0.60}FA_{0.40}PbI_{3-y}Cl_y$-a week later (turquoise) thin films.

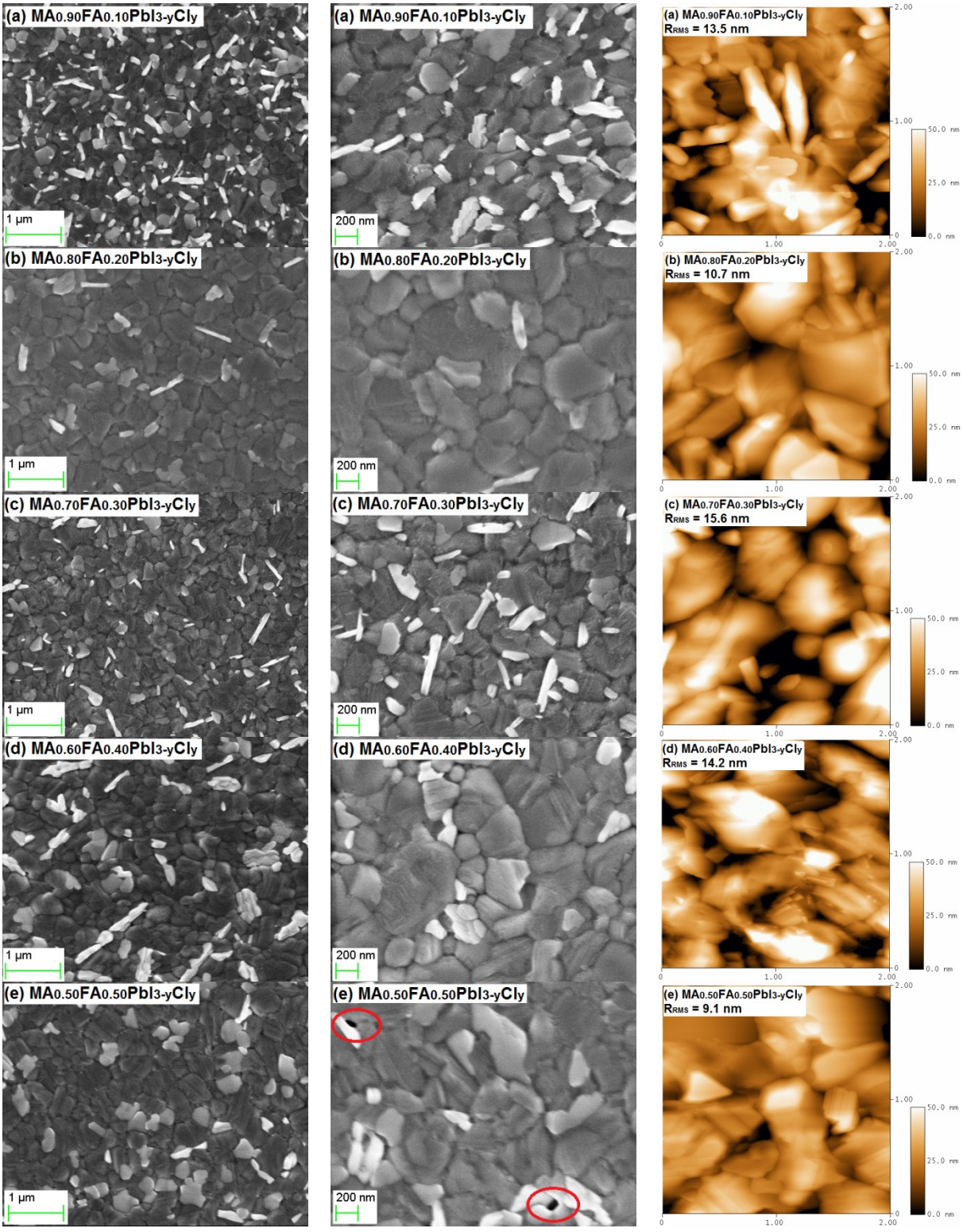

Fig. S7. The SEM and AFM images of (a) $MA_{0.90}FA_{0.10}PbI_{3-y}Cl_y$, (b) $MA_{0.80}FA_{0.20}PbI_{3-y}Cl_y$, (c) $MA_{0.70}FA_{0.30}PbI_{3-y}Cl_y$, (d) $MA_{0.60}FA_{0.40}PbI_{3-y}Cl_y$, and (e) $MA_{0.50}FA_{0.50}PbI_{3-y}Cl_y$ thin films annealed at 100 °C. The SEM scale bars are 1 μm (left) and 200 nm (middle). The AFM scale is 2 μm and height scale bar is 50 nm. R_{RMS} values are indicated on the AFM images (right). Pinhole formations are highlightened by the red circles.

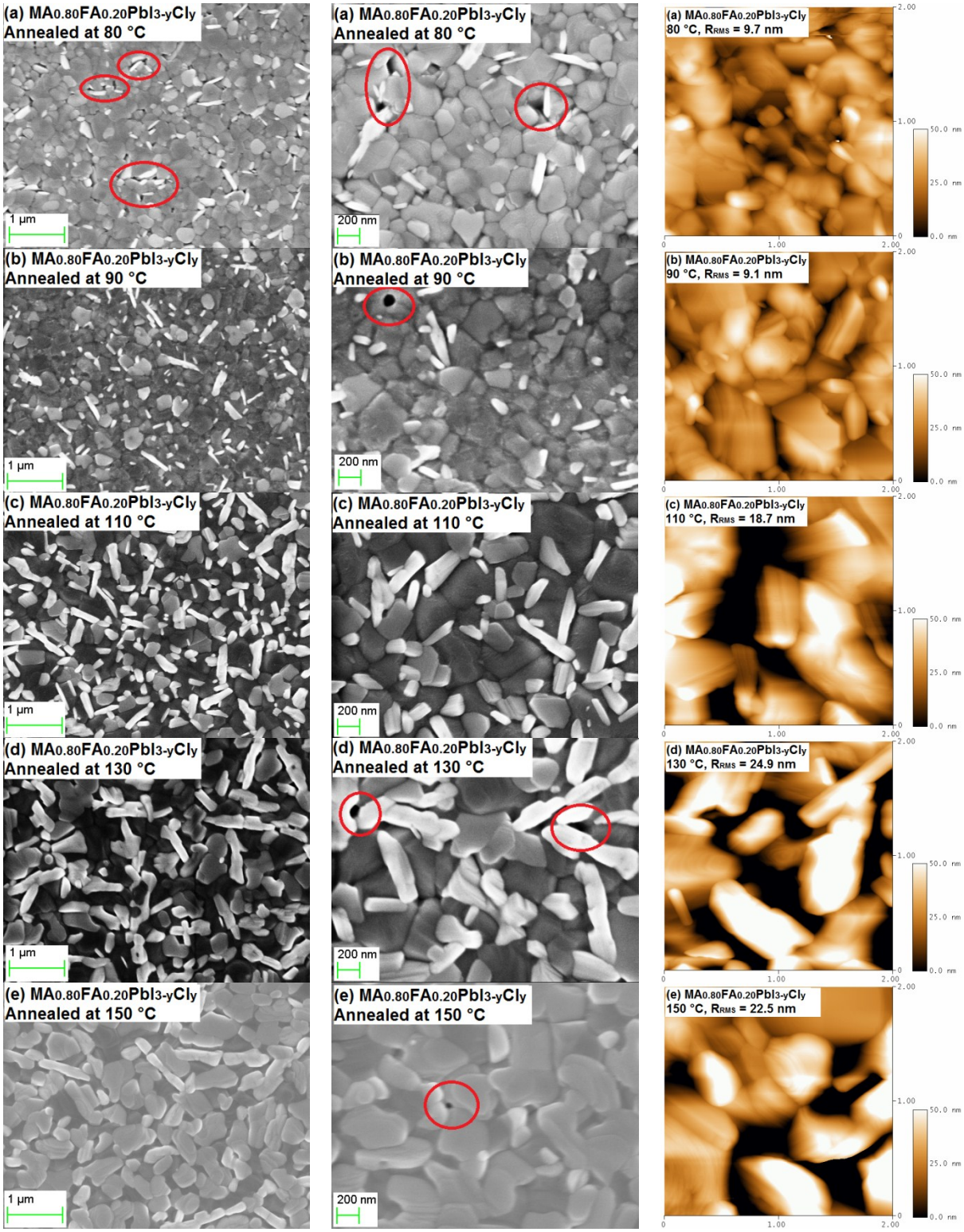

Fig. S8. The SEM and AFM images of $MA_{0.80}FA_{0.20}PbI_{3-y}Cl_y$ thin films annealed at (a) 80 °C, (b) 90 °C, (c) 110 °C, (d) 130 °C, and (e) 150 °C. The SEM scale bars are 1 μm (left) and 200 nm (middle). The AFM scale is 2 μm and height scale bar is 50 nm. R_{RMS} values are indicated on the AFM images (right). Pinhole formations are highlightened by the red circles.

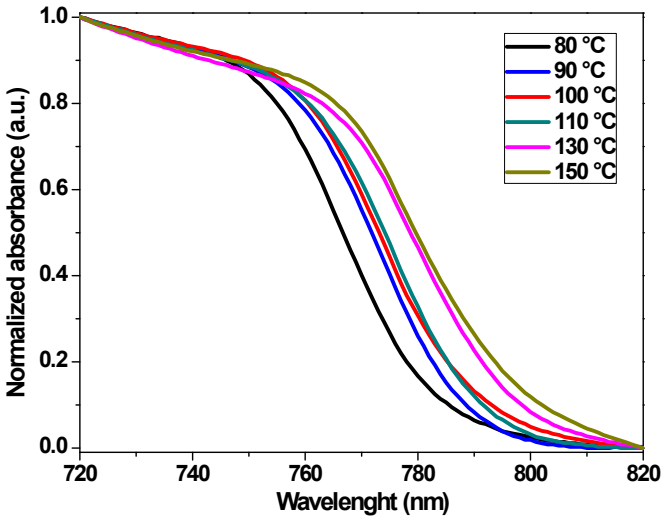

Fig. S9. UV-Vis absorption spectra of $MA_{0.80}FA_{0.20}PbI_{3-y}Cl_y$ films annealed at different temperatures.

Eq. S2. The carrier diffusion lengths are calculated according to the 1D diffusion model which is well described in the study of Xing *et al*.[4] In this model, temporal total charge number *N*(t) is defined as:

$$N(t) = \frac{2n_0 L}{\pi} exp(-kt) \sum_{m=0}^{\infty} \left(exp(-\frac{\pi^2 D}{L^2}(m+\frac{1}{2})^2 t) \frac{\exp(-\alpha L)\pi\left(m+\frac{1}{2}\right) + (-1)^m \alpha L}{((\alpha L)^2 + \pi^2\left(m+\frac{1}{2}\right)^2)(m+\frac{1}{2})} \right)$$

L is the thickness of the perovskite thin films, *k* is the PL decay rate in the absence of quenchers.

Supplementary references:

1. S. Brittman, G. W. Adhyaksa and E. C. Garnett, *MRS Commun.*, **2015**, 5, 7-26.
2. I. Swainson, L. Chi, J.-H. Her, L. Cranswick, P. Stephens, B. Winkler, D. J. Wilson and V. Milman, *Acta Crystallogr. Sect. B-Struct. Sci.*, **2010**, 66, 422-429.
3. J. M. Frost, K. T. Butler, F. Brivio, C. H. Hendon, M. van Schilfgaarde and A. Walsh, *Nano Lett.*, **2014**, 14, 2584-2590.
4. G. Xing, N. Mathews, S. Sun, S. S. Lim, Y. M. Lam, M. Grätzel, S. Mhaisalkar and T. C. Sum, *Science*, **2013**, 342, 344-347.